THE JOURNAL OF PHYSICAL CHEMISTRY LETTERS
A JOURNAL OF THE AMERICAN CHEMICAL SOCIETY

pubs.acs.org/JPCL

Letter

Mesoporous Silica Encapsulated Platinum−Tin Intermetallic Nanoparticles Catalyze Hydrogenation with an Unprecedented 20% Pairwise Selectivity for Parahydrogen Enhanced Nuclear Magnetic Resonance

Yong Du, Ranjan K. Behera, Raghu V. Maligal-Ganesh, Minda Chen, Tommy Yunpu Zhao, Wenyu Huang,* and Clifford R. Bowers*

Cite This: *J. Phys. Chem. Lett.* 2022, 13, 4125−4132

Read Online

ACCESS | Metrics & More | Article Recommendations | Supporting Information

ABSTRACT: Supported noble metals offer key advantages over homogeneous catalysts for in vivo applications of parahydrogen-based hyperpolarization. However, their performance is compromised by randomization of parahydrogen spin order resulting from rapid hydrogen adatom diffusion. The diffusion on Pt surfaces can be suppressed by introduction of Sn to form Pt−Sn intermetallic phases. Herein, an unprecedented pairwise selectivity of 19.7 ± 1.1% in the heterogeneous hydrogenation of propyne using silica encapsulated Pt−Sn intermetallic nanoparticles is reported. This high level of selectivity exceeds that of all supported metal catalysts by at least a factor of 3. Moreover, the pairwise selectivity for alkyne hydrogenation is about 2 times higher than for alkene hydrogenation, an observation attributed to the higher coverage of the former and its effect on diffusion. Lastly, $PtSn@mSiO_2$ nanoparticles exhibited improved coking resistance, and any loss of activity is shown to be fully reversible through high-temperature oxidation−reduction cycling.

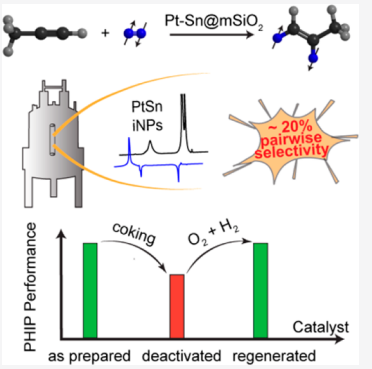

Parahydrogen-based hyperpolarization is an efficient and inexpensive method for sensitivity enhanced NMR spectroscopy and imaging.[1−3] Conversion of the proton singlet spin order of parahydrogen ($p\text{-}H_2$) into NMR observable hyperpolarization is mediated by chemical hydrogenation into magnetically inequivalent sites, resulting in high-field proton NMR signal enhancements that can in theory exceed 4 orders of magnitude. An essential requirement of parahydrogen-based hyperpolarization is pairwise addition, where the pair of H atoms that are incorporated into the hydrogenation adduct originate from the same $p\text{-}H_2$ molecule. Parahydrogen enhanced NMR by heterogeneous catalysis would be highly suitable for in vivo applications, where the hyperpolarized reaction products are readily separable from the insoluble solid catalyst material. However, the maximum reported pairwise selectivity for a monometallic supported nanoparticle catalyst is around 6−7% for hydrogenation of propene over highly dispersed Rh/TiO_2 or atomically dispersed Pt/CeO_2.[4,5]

Incorporating a promoter metal such as Sn to form Pt−Sn bimetallic NPs can improve selectivity for many reactions,[6−8] including hydrogenations, and can also suppress C−C bond cleavage that leads to carbon deposition and catalyst deactivation.[7,9] These effects have been ascribed to the lowering of the adsorption energy of the hydrocarbons and have been studied by temperature-programmed desorption (TPD),[10] Auger electron spectroscopy (AES),[10] low-energy electron diffraction (LEED),[6,7,10−15] and density functional theory (DFT).[16−18] The intermetallic phases in the present work were obtained by seeded growth and high-temperature annealing at 600 °C within a protective mesoporous silica ($mSiO_2$) shell.[19] In experiments with $p\text{-}H_2$, the surface structure of Pt−Sn intermetallic nanoparticles (iNPs) has played a role in several extraordinary spin polarization phenomena. $Pt_3Sn@mSiO_2$ iNPs were shown to mediate conversion of $p\text{-}H_2$ singlet order into hyperpolarization of liquid water and alcohols,[20] and $PtSn@mSiO_2$ iNPs were previously shown to catalyze hydrogenation of propene (PE) to propane (PA) with a high pairwise selectivity of 10%.[21] Remarkably, $PtSn@mSiO_2$ iNPs exhibited a 3000-fold higher pairwise selectivity relative to similarly sized monometallic $Pt@mSiO_2$ NPs. A key difference between the two is the absence of 3-fold Pt(111) hollow sites on PtSn. These sites have been implicated in the facile H_2 dissociation[22−24] and fast H adatom diffusion on Pt(111) surfaces where such sites are contiguous.

In the literature, significant differences in conversion and pairwise selectivity have been observed in the hydrogenation of

Received: February 27, 2022
Accepted: April 15, 2022
Published: May 4, 2022

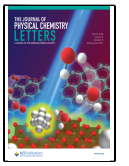

https://doi.org/10.1021/acs.jpclett.2c00581
J. Phys. Chem. Lett. 2022, 13, 4125−4132

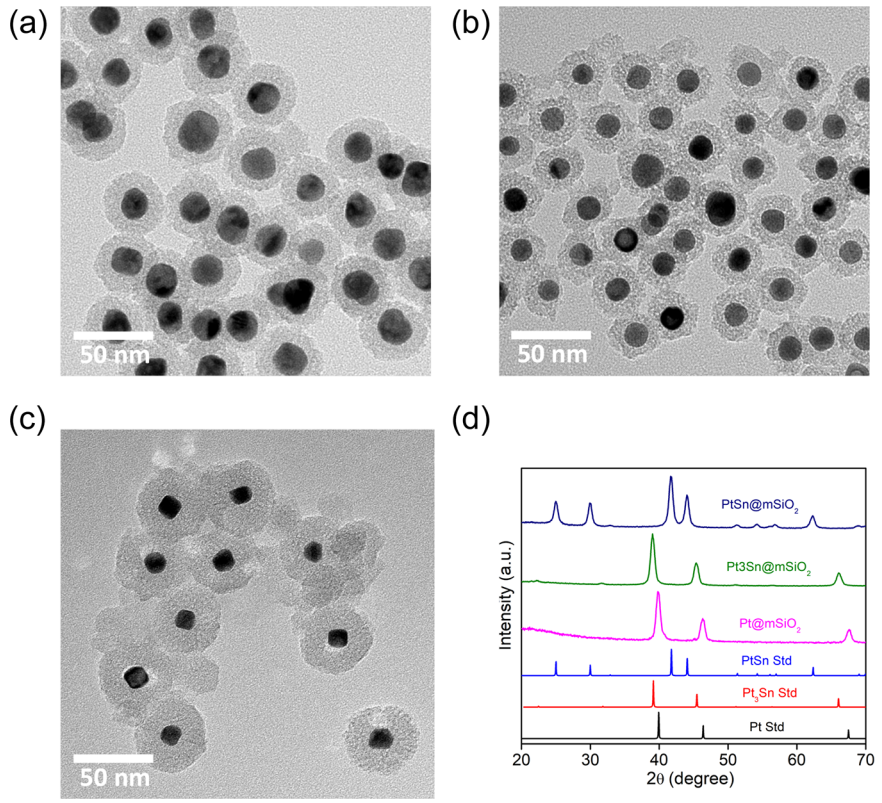

Figure 1. TEM images of (A) $PtSn@mSiO_2$, (B) $Pt_3Sn@mSiO_2$, and (C) $Pt@mSiO_2$ NPs and (D) PXRD patterns.

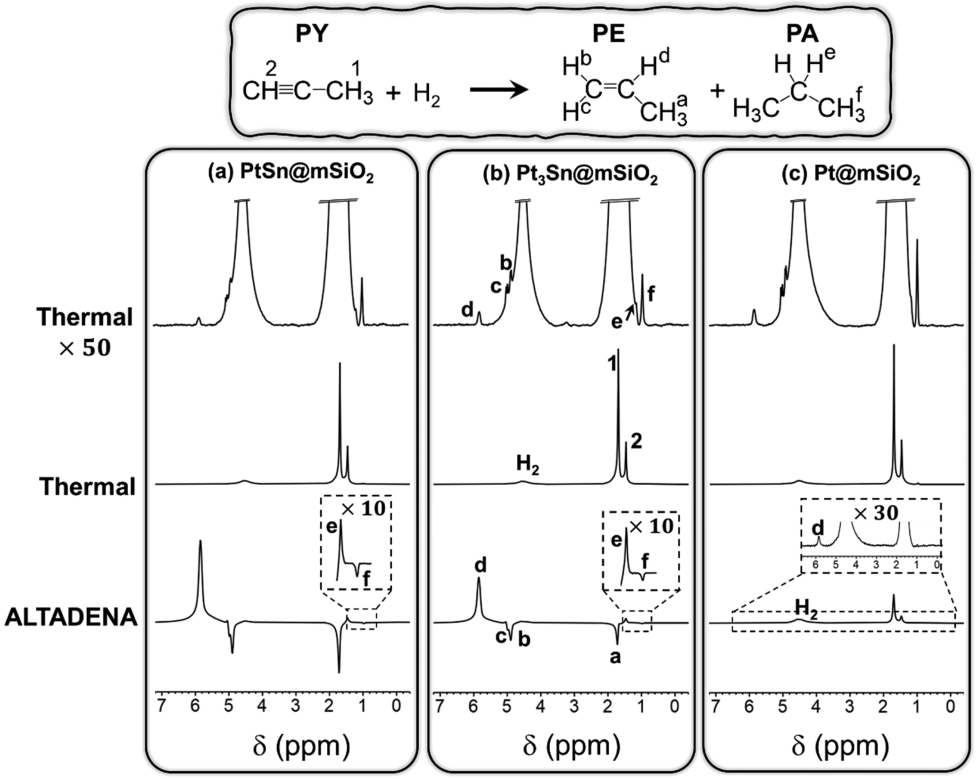

Figure 2. Thermally polarized (top: ×50 and middle) and ALTADENA (bottom) ^1H NMR spectra of reaction effluent in propyne hydrogenation with 50% p-H_2 over 15 mg of (a) $PtSn@mSiO_2$, (b) $Pt_3Sn@mSiO_2$, and (c) $Pt@mSiO_2$ at 250 °C. The insets in the dashed frame are the vertically expanded propane $-CH_2$ and $-CH_3$ peaks (e and f). The reactant gas consisted of 120/70/210 mL/min of H_2/N_2/propyne.

alkynes vs alkenes over the same catalysts. For instance, an increase in the signal enhancement by an order of magnitude was reported in the hydrogenation of propyne (PY) compared to hydrogenation of PE using a silica-supported vanadium oxo

https://doi.org/10.1021/acs.jpclett.2c00581
J. Phys. Chem. Lett. 2022, 13, 4125−4132

organometallic catalyst.[25] Similar observations were reported for other catalytic systems such as immobilized iridium complexes[26] and silica/alumina/zirconia supported Pd NPs.[27] The present study of PY hydrogenation was aimed at exploring the potentially higher performance, in terms of both conversion and pairwise selectivity, that may be achieved for the alkyne hydrogenation over the Pt_3Sn and PtSn iNPs. High-resolution transmission electron microscopy (TEM) images and powder X-ray diffraction patterns (PXRD) of Pt@mSiO_2, Pt_3Sn@mSiO_2, and PtSn@mSiO_2 NPs are presented in Figure 1.

In the ALTADENA experiment,[28] hydrogenation with p-H_2 is performed near zero magnetic field followed by transport of the products under adiabatic passage conditions to high field for NMR detection. In our experiments, the U-tube reactor was positioned in the 5 mT fringe field of the 9.4 T Bruker Ultrashield superconducting magnet, and transport occurred via gas flow through tubing connecting the outlet of the U-tube and the detection coil of the NMR probe. Further details are provided in the Experimental Methods section.

Figure 2 presents the 400 MHz ^{1}H ALTADENA NMR spectra of the reactor effluent in the hydrogenation of PY with 50% p-H_2 at a reactor temperature of 250 °C. The corresponding spectra acquired after allowing the nuclear spins to fully relax to thermal equilibrium are also presented. The signal enhancement factor is defined as the ratio of the ALTADENA and thermal equilibrium NMR signals after each is divided by its respective number of accumulated transients. The pairwise selectivity is estimated as the ratio of the observed and theoretical enhancement factors.[29] The formulas are included in the Supporting Information. In the ALTADENA spectra, the PE $-CH^d$ proton and one of the PE $-CH_2$ protons, either H^b for *syn*-addition or H^c for *anti*-addition, originate from p-H_2. Notably, the PE $-CH_3$ group signal (peak "a") is very intense, with an absolute intensity similar to that of $-CH^d$, even though no methyl protons originated from p-H_2. This sharing of p-H_2 spin order stems from a combination of two effects: (1) mixing of the methyl proton spin states into the low field eigenstates incorporating the p-H_2 protons and (2) transfer of spin order resulting from the rapid adiabatic transport through level anticrossings induced by proton−proton spin coupling. Therefore, to calculate the pairwise selectivity from the enhancement factor for a specific proton peak, the theoretical enhancement factor for that site needs to be known. Density matrix simulations[30] (see the Supporting Information) show that the enhancement factor for the PE $-CH^d$ proton depends on the stereochemistry of addition to PY. The ^{1}H signal enhancement factors for pure *syn*- or *anti*-addition of 50% p-H_2 are calculated to be 5175 and 8072, respectively, at 9.4 T and 298 K. Hence, quantitation of the stereoselectivity is necessary for the accurate estimate of the pairwise selectivity. Because *syn*- and *anti*-addition yield distinct PE ALTADENA spectral features (Figure S1), the stereoselectivity can be estimated by fitting the experimental spectrum to a linear combination of simulated *syn*- and *anti*-addition ALTADENA spectra.[31]

The spectral fitting, shown in Figure S2, indicates a stereoselectivity of 69 ± 2% *syn*-addition for PtSn@mSiO_2 at 250 °C, corresponding to a theoretical enhancement factor of 6073 ± 58 for H^d. For the same catalyst, the maximum experimentally measured signal enhancement factor was 1198 ± 67 after correction for spin−lattice relaxation losses during transport from the U-tube to the NMR probe (see the Supporting Information for details). Hence, the pairwise selectivity is 19.7 ± 1.1% (15.8% uncorrected). This is the highest pairwise selectivity to be reported for a supported metal catalyst in a gas/solid heterogeneous reaction.

Figure 3a,b compares the observed signal enhancements for PE and PA and the corresponding pairwise selectivities for all

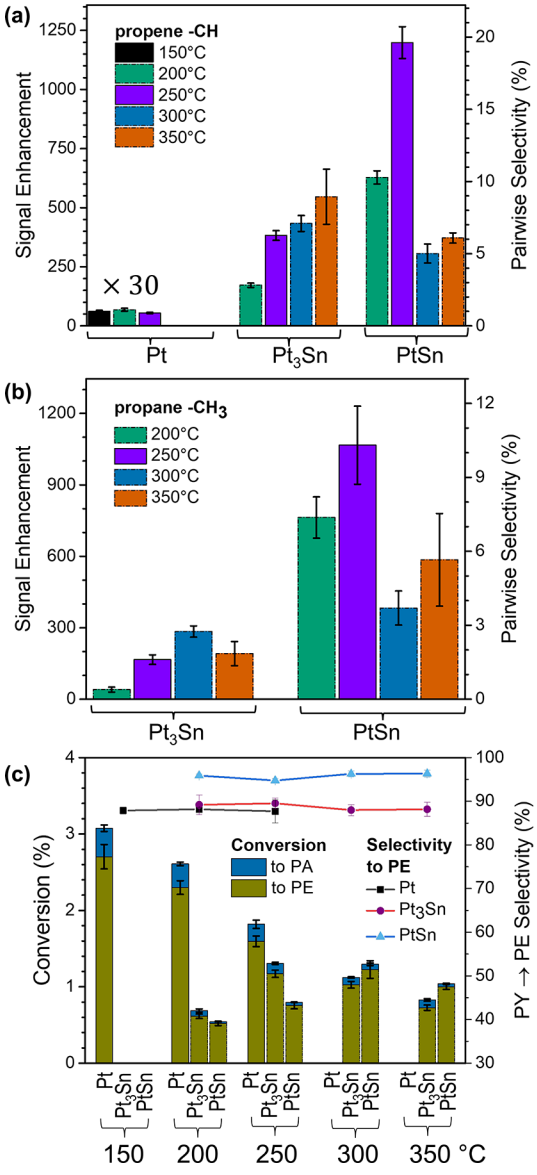

Figure 3. (a) Propene −CH peak and (b) propane $-CH_3$ peak signal enhancement factors and pairwise selectivity in the hydrogenation of propyne over Pt@mSiO_2, Pt_3Sn@mSiO_2, and PtSn@mSiO_2 at temperatures from 150 to 350 °C. (c) Partial hydrogenation selectivity and percent conversions to propene and propane.

three catalysts at temperatures ranging from 150 to 350 °C. Consistent with the results for PE hydrogenation,[21] introduction of Sn to form the intermetallic phase drastically affects the signal enhancements of both PE and PA. Compared to the 1198-fold enhancement obtained for PtSn@mSiO_2 at 250 °C, Pt_3Sn@mSiO_2 and Pt@mSiO_2 afforded much lower PE $-CH^d$ peak signal enhancement factors of 382, and 2, respectively, at the same temperature.

Hyperpolarized and thermally polarized PA peaks ("e" and "f") were also detected with pairwise selectivities of 10.3%,

https://doi.org/10.1021/acs.jpclett.2c00581
J. Phys. Chem. Lett. 2022, 13, 4125−4132

1.6%, and 0% for PtSn, Pt_3Sn, and Pt at 250 °C, respectively. The 10.3% pairwise selectivity of PtSn@$mSiO_2$ is similar to the value obtained in our previous study of PE hydrogenation with this catalyst.[21] The full data set with experimental uncertainties for the three catalysts is provided in Figures S3 and S4 as well as Tables S3−S6.

The percentage conversions of PY to PE and PA for the three catalysts are reported in Figure 3c. For Pt@$mSiO_2$, conversion decreased monotonically with temperature, and hydrogenation products could not be detected at temperatures over 300 °C. For PtSn@$mSiO_2$ and Pt_3Sn@$mSiO_2$ iNPs, conversion initially increased with temperature but eventually decreased slightly at higher temperatures. PY to PE conversion followed the order Pt@$mSiO_2$ > Pt_3Sn@$mSiO_2$ > PtSn@$mSiO_2$, while the pairwise selectivity exhibits the reverse trend. Such an inverse relationship was reported in the hydrogenation of PE to PA for this series of three catalysts.[21] However, conversion of PY was about a factor of 4 greater than the conversion of PE for the same PtSn@$mSiO_2$ catalyst.[21] Notably, the variation in conversion with the mole fraction of Sn was smaller for hydrogenation of PY relative to PE. Pt@$mSiO_2$ and Pt_3Sn@$mSiO_2$ exhibited significantly lower conversion for PY as the reactant (1−3%) compared to 15−25% for PE.

The observed trends in conversion and signal enhancement as a function of the fraction of Sn in the catalyst can be rationalized based on literature studies of molecular adsorption and diffusion on Pt−Sn surface alloys.

Effect on Density of Adsorbed PY. TPD measurements show that the adsorption energy of PY decreases from 161 kJ/mol on Pt(111) to 119 kJ/mol on p(2 × 2) Pt_3Sn(111) to 96 kJ/mol on $(\sqrt{3} \times \sqrt{3})$ $R30°$ Pt_2Sn(111),[10] where the surface overlayer structure is specified by using Wood's notation. Therefore, the density of adsorbed PY is expected to decrease as the Sn fraction increases, thereby lowering conversion. Pairwise selectivity for alkyne hydrogenation was about a factor of 2 higher than for alkene hydrogenation. Because of the much stronger adsorption of the alkyne compared to H_2, the metal surface is almost completely covered by PY molecules, and H_2 can only be adsorbed within the interspace between them, which can be expected to further hinder H adatom diffusion.

Effect on H Adatom Density. Dissociative D_2 chemisorption on Pt/Sn alloys has been studied by hyperthermal molecular beam experiments. On Pt(111) surfaces, the activation energy barrier of D_2 dissociation was reported to be 2 kJ/mol, while a slightly higher barrier was observed on p(2 × 2) Pt_3Sn(111) surface.[24,32] On $(\sqrt{3} \times \sqrt{3})$ $R30°$ Pt_2Sn(111), the barrier increased to 27 kJ/mol. Inhibition of dissociative H_2 chemisorption reduces the H adatom density, contributing to the lower conversions observed on PtSn iNPs. Moreover, a TPD study demonstrated that the saturation coverage of D adatoms decreases from 0.95 monolayer (ML) on Pt(111) to 0.68 ML on p(2 × 2) Pt_3Sn(111) and 0.51 ML on $(\sqrt{3} \times \sqrt{3})$ $R30°$ Pt_2Sn(111) at 110 K.[23] For PtSn iNPs, the absence of 3-fold Pt_3 hollow sites is expected to further decrease coverage and conversion.[24]

Effect on Direct Addition of Molecular H_2. Because of the high barrier to dissociate H_2 molecules on PtSn (ca. 29 kJ/mol),[19] the fraction of adducts formed by direct addition of molecular H_2 is expected to be higher on this surface. In direct addition, both H atoms in molecular H_2 approach the carbon−carbon triple bond from the same side in a reaction path favoring concerted, pairwise hydrogenation.[21]

Effect on the Activation Energy Barrier of H Adatom Diffusion. The activation energy of H adatom diffusion increases with increasing Sn content due to the loss of 3-fold Pt_3 hollow sites where high coordination Pt_3−H binding occurs.[24] The DFT study by Fearon and Watson indicates that the maximum energy barriers of hydrogen diffusion on Pt(111), p(2 × 2) Pt_3Sn(111), and $(\sqrt{3} \times \sqrt{3})$ $R30°$ Pt_2Sn(111) are 5, 41, and 100 kJ/mol, respectively (PtSn (110) was not included in that study).[22] By restricting diffusion, the lifetime of proton singlet spin order on H adatom pairs is prolonged. For the fraction of hydrogenation adducts formed by stepwise addition, elevation of the barrier to H adatom diffusion on Pt−Sn surfaces will have the effect of increasing the pairwise selectivity. This picture is consistent with an experimental para−ortho H_2 back-conversion flow study,[20] which revealed that para−ortho back-conversion is negligible below 200 °C on PtSn@$mSiO_2$. The decrease in pairwise selectivity above 250 °C is consistent with increased dissociation of H_2 on PtSn@$mSiO_2$ iNPs at higher temperatures.

As seen in Figure 3c, the partial hydrogenation selectivity (PHS) to PE was >87% for all three catalysts. Similarly high PHS was reported for alkyne hydrogenations on Pd catalysts.[27,33,34] The PE produced from partial hydrogenation has a lower adsorption energy than that of PY, resulting in PE replacement by PY in the feed.[34] This is also evidenced by a TPD study of Pt(111), p(2 × 2) Pt_3Sn(111), and $(\sqrt{3} \times \sqrt{3})$ $R30°$ Pt_2Sn(111) showing that the adsorption energy decreases from 161, 119, and 96 kJ/mol for PY to 73, 62, and 49 kJ/mol for PE, respectively.[10,13] Of the three catalysts, PtSn@$mSiO_2$ achieved the highest PHS of 95% at all temperatures, while lower PHS values were recorded for Pt_3Sn and Pt NPs. The PHS of the three catalysts may also be affected by differences in the H_2 dissociation. As noted above, the density of H adatoms on the PtSn catalysts will be reduced because of the higher barrier of H_2 dissociation, thus inhibiting the over-hydrogenation to PA.

Activity loss was observed in experiments with all three catalysts at elevated temperatures and is attributed to accumulation of carbonaceous deposits.[35,36] DFT studies indicate that the onset of C−C scission on the Pt(111) surface proceeds through PY due to its relatively strong adsorption and large exothermicity compared to other C_3H_x (x = 3−8) hydrocarbons.[17] Moreover, Peck et al. reported that ∼80% of chemisorbed PY on Pt (111) undergoes decomposition to form surface carbons by post-TPD AES experiments.[10] However, the incorporation of Sn in Pt/Sn alloys can delay the progression toward deactivation. In this study, the conversion of PY to PE started to decline at 150, 250, and 350 °C on Pt@$mSiO_2$, Pt_3Sn@$mSiO_2$, and PtSn@$mSiO_2$, respectively (Figure 3c and Figure S5). This demonstrates that the incorporation of Sn can effectively reduce but not eliminate the deactivation due to coke formation.[37,38]

Methods for catalyst regeneration to restore the activity of spent Pt−Sn alloys have been extensively investigated .[37,39,40] A typical regeneration procedure consists of exposing used catalysts to O_2 or air at high temperatures to burn off the carbonaceous deposits followed by a reduction in H_2.[39,41,42] In the present work, to examine if the performance of three Pt−Sn@$mSiO_2$ NPs is recovered after vigorous PY hydrogenation

https://doi.org/10.1021/acs.jpclett.2c00581
J. Phys. Chem. Lett. 2022, 13, 4125−4132

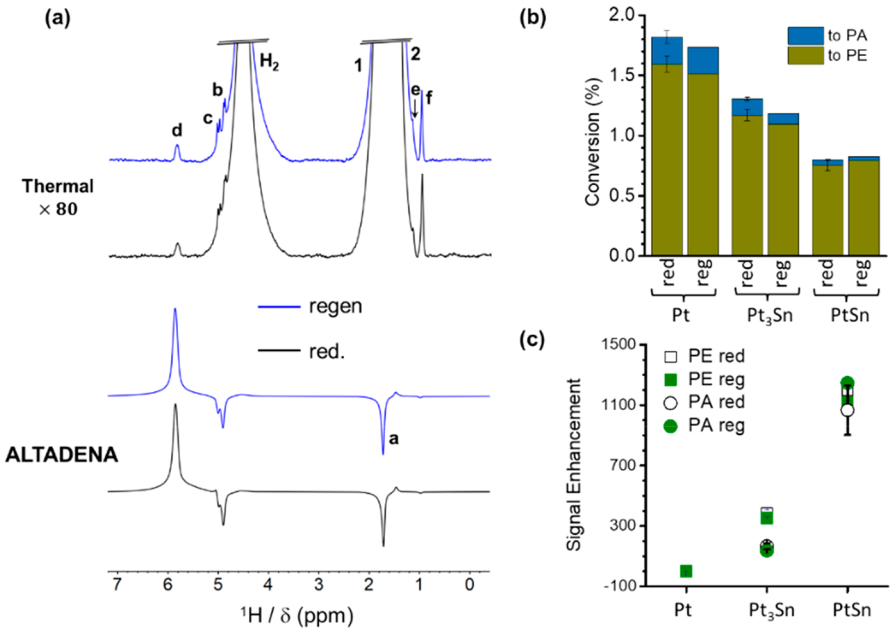

Figure 4. (a) Thermal and ALTADENA spectra acquired after initial reduction (red) and after regeneration (reg) of spent $PtSn@mSiO_2$ catalyst. (b) Percent conversions and (c) signal enhancement factors in the hydrogenation of propyne over $Pt@mSiO_2$, $Pt_3Sn@mSiO_2$, and $PtSn@mSiO_2$ at 250 °C after two catalysts treatments: (1) initial reduction in H_2 at 600 °C and (2) regeneration, consisting of oxidation in the air at 500 °C followed by a reduction in H_2 at 600 °C.

runs, a similar oxidation−reduction cycling regeneration approach was employed. The spent Pt, Pt_3Sn, and PtSn catalysts were heated under continuous air flow at 500 °C for 2 h followed by a reduction in H_2 at 600 °C for 2 h. As shown in Figure 4, no significant difference in conversion or NMR signal enhancement factor was observed for all three catalysts except for a slight reduction in PE −CH signal enhancement on $PtSn@mSiO_2$ after the regeneration as compared to the initial runs (i.e., 1198 vs 1121). The measured values for the conversions, signal enhancement factors, and pairwise selectivities of three NPs after the oxidation−reduction cycling are summarized in Figure S6 and Table S7. The restoration in the performance of three NPs is likely due to the removal of surface carbon deposits during the catalyst regeneration process.[43−46] Thus, $Pt_3Sn@mSiO_2$ and $PtSn@mSiO_2$ iNPs are robust and effective catalysts for achieving high NMR signal enhancement with excellent durability and recyclability in parahydrogen enhanced NMR. For these catalysts, the $mSiO_2$ shell effectively prevents the encapsulated iNPs from aggregation at high temperatures.

To summarize, conversion of PY to PE followed the trend $Pt@mSiO_2$ > $Pt_3Sn@mSiO_2$ > $PtSn@mSiO_2$ while signal enhancement (and pairwise selectivity) followed the reverse order. The same trends were observed for the hydrogenation of PE to PA in ref 21. The $PtSn@mSiO_2$ iNPs exhibited a 19.7 ± 1.1% pairwise selectivity in the hydrogenation of PY to PE at 250 °C, which is the highest pairwise selectivity to be observed for a supported metal nanoparticle catalyst. In contrast, similarly sized $Pt@mSiO_2$ NPs exhibited a maximum pairwise selectivity of only 0.04%. The main difference between the Pt and PtSn surfaces is the occurrence of contiguous 3-fold Pt sites on the former. These sites have been implicated in the facile H_2 dissociation and H adatom diffusion on Pt(111) surfaces. Restriction of diffusion will prolong the lifetime of singlet spin order in an H adatom pair originating from a p-H_2 molecule. Direct addition of molecular H_2, which is inherently pairwise, can also explain the high pairwise selectivity observed for the PtSn catalyst. The hypothesis for direct molecular addition is supported by the results of a para−ortho H_2 back-conversion flow study in ref 20, which showed that temperatures above 200 °C are necessary to activate para−ortho conversion on $PtSn@mSiO_2$ iNPs. The decrease in pairwise selectivity above 250 °C is consistent with increased H_2 dissociation on $PtSn@mSiO_2$ iNPs at elevated temperatures. Because the observed pairwise selectivity of PY hydrogenation is well below 100%, it appears that a substantial fraction of adducts are formed by stepwise addition. Therefore, the possibility of significant parallel contributions from both paths cannot be excluded.

PY hydrogenation was found to occur with nearly twice the pairwise selectivity as PE hydrogenation. We hypothesize that this is due to the higher coverage of the former and the resulting restriction of diffusion. The relatively low conversion of PY hydrogenation using 15 mg of $PtSn@mSiO_2$ (ca. 1%) is not unexpected given the high 400 mL/min flow rate used in the present work, which is necessary to avoid spin relaxation during transport to the NMR probe. Under these conditions, even the conversion using $Pt@mSiO_2$ was only 2−3%.

Hyperpolarized gaseous alkenes produced by continuous-flow hydrogenation with parahydrogen could have interesting prospective applications. For example, they could be employed as hyperpolarized reactants for sensitivity enhanced NMR studies of downstream catalytic transformations, not limited to hydrogenation. Another possibility is to use the hyperpolarized alkenes in sensitivity enhanced operando NMR spectroscopy of alkene adsorption, surface interactions, and chemical transformations. Spin order transfer of proton hyperpolarization on the adsorbed alkene to other chemical species, including nuclear spins at active sites of catalysts, could widen the scope of such an approach.

Finally, we demonstrated that the activity of the silica encapsulated catalysts, which is diminished at higher temper-

https://doi.org/10.1021/acs.jpclett.2c00581
J. Phys. Chem. Lett. 2022, 13, 4125−4132

atures due to the formation of carbonaceous deposits, can be readily recovered by the oxidation−reduction cycling, which proves that the activity loss is not due to surface reconstruction or phase separation. With the advantages of high activity, selectivity, stability, and the ease of separation from the hydrogenation products, the Pt−Sn@mSiO$_2$ iNPs materials provide an attractive catalytic platform for producing hyperpolarized gases and liquids.

EXPERIMENTAL METHODS

Platinum and Platinum−Tin Nanoparticles. Details of the syntheses of Pt@mSiO$_2$ and Pt−Sn@mSiO$_2$ NPs have been published previously[8] and are also included in the Supporting Information. Briefly, the core−shell structured Pt@mSiO$_2$ NPs were synthesized by using tetradecyltrimethylammonium bromide-capped (TTAB-capped) Pt NPs as initial core material for the subsequent silica polymerization with tetraethyl orthosilicate (TEOS), followed by removal of TTAB molecules in the calcination. The intermetallic phases of PtSn and Pt$_3$Sn were prepared by heterogeneous nucleation of Sn from SnCl$_2$·2H$_2$O at the metal surface of Pt@mSiO$_2$ in tetraethylene glycol. The metal loadings, particle sizes, Pt dispersion, and the surface site densities of three NPs are summarized in Table S1. Additional characterizations of the three catalysts are presented in the Supporting Information and in previous publications.[8,21]

Hydrogenation. Hydrogen enriched to 50% p-H$_2$ was prepared by flowing normal ultrahigh purity H$_2$ gas through a liquid nitrogen cooled coiled copper tube (0.25 in. O.D.) containing iron oxide hydroxide, as described elsewhere.[47] Hydrogenation of gaseous PY was performed under ALTADENA[28] conditions where the reaction is performed in the fringe field of the 9.4 T Bruker Avance Ultrashield superconducting magnet, and the reactor effluent containing products and unreacted reactants is transported by flow to a standard Bruker 10 mm liquids probe for NMR detection at 400 MHz. The reaction mixture containing H$_2$ and PY as reactants and N$_2$ as a dilutant buffer gas was premixed by combining the outputs of three mass flow controllers (Alicat Scientific) set to flow rates of 120/210/70 mL/min. The mixture was fed into a U-shaped quartz tube (0.25 in. O.D.; 0.15 in. I.D.) reactor packed with 15 mg of Pt@mSiO$_2$, Pt$_3$Sn@mSiO$_2$, or PtSn@mSiO$_2$ catalysts. The catalyst was held in place with quartz wool. The temperature in the reactor U-tube was regulated by a home-built temperature controller with feedback from a K-type thermocouple inserted directly into the catalyst bed. The gaseous reactor effluent flowed through PFA tubing (0.125 in. O.D.; 0.0625 in. I.D.; 1 m length) and was delivered through a thin glass capillary to the bottom of a 10 mm O.D. NMR tube inserted into the NMR probe. ALTADENA mode NMR spectra were collected by accumulating 64 free induction decays with a 2 s recycle delay with gases flowing continuously. For each catalyst, the hydrogenation reaction was repeated by using n-H$_2$. Thermally polarized spectra at Boltzmann equilibrium were acquired by accumulating 512 free induction decays with a recycle delay of 6 s under the nonflowing condition with the gas effluent sealed in the NMR sample loop. The spectra were processed by using MestReNova ver. 14.2 software, and the signal integrals of the propene −CH, propane −CH$_3$, and propyne −CH peaks of the ALTADENA and thermally polarized NMR spectra were obtained by multipeak fitting. The peak height, line width, and Lorentzian/Gaussian ratio were varied to optimize the fit while the chemical shifts were fixed.[25]

Catalyst Treatments. Two different catalyst activation treatments were employed in the present work. Freshly synthesized Pt$_3$Sn and PtSn catalysts were reduced at 600 °C and Pt catalysts at 300 °C in a stream of 90/10 mL/min of N$_2$/H$_2$ for 2 h before performing hydrogenation reactions. Regeneration treatments on spent catalysts consisted of oxidation−reduction cycling and were performed after catalyst deactivation at higher reaction temperatures. To restore the activity of the Pt−Sn@mSiO$_2$ iNPs, the catalyst was oxidized with 50 mL/min of air at 500 °C for 2 h, followed by the reduction with 90/10 mL/min of N$_2$/H$_2$ at 600 °C for 2 h. In both catalyst treatments, the hydrogenation reactor was cooled to room temperature prior to starting the hydrogenation reactions.

ASSOCIATED CONTENT

Supporting Information

The Supporting Information is available free of charge at https://pubs.acs.org/doi/10.1021/acs.jpclett.2c00581.

Information about the catalyst synthesis and characterization, catalyst turnover frequencies, numerical density matrix simulations details, formulas used for calculation of the conversion, pairwise selectivity, spectral fitting, and NMR signal enhancement, as well as tabulated numerical values for these values at all temperature studied; the complete set of all ALTADENA and thermal equilibrium experimental spectra that were acquired in this study (PDF)

AUTHOR INFORMATION

Corresponding Authors

Clifford R. Bowers − *Department of Chemistry and National High Magnetic Field Laboratory, University of Florida, Gainesville, Florida 32611, United States;* orcid.org/0000-0001-6155-5163; Email: bowers@chem.ufl.edu

Wenyu Huang − *Department of Chemistry, Iowa State University, Ames, Iowa 50011, United States; Ames Laboratory, U.S. Department of Energy, Ames, Iowa 50011, United States;* orcid.org/0000-0003-2327-7259; Email: whuang@iastate.edu

Authors

Yong Du − *Department of Chemistry and National High Magnetic Field Laboratory, University of Florida, Gainesville, Florida 32611, United States*

Ranjan K. Behera − *Department of Chemistry, Iowa State University, Ames, Iowa 50011, United States*

Raghu V. Maligal-Ganesh − *Department of Chemistry, Iowa State University, Ames, Iowa 50011, United States;* orcid.org/0000-0001-8332-4454

Minda Chen − *Department of Chemistry, Iowa State University, Ames, Iowa 50011, United States;* orcid.org/0000-0002-9881-9350

Tommy Yunpu Zhao − *Department of Chemistry and National High Magnetic Field Laboratory, University of Florida, Gainesville, Florida 32611, United States*

Complete contact information is available at: https://pubs.acs.org/10.1021/acs.jpclett.2c00581

https://doi.org/10.1021/acs.jpclett.2c00581
J. Phys. Chem. Lett. 2022, 13, 4125−4132

Notes

The authors declare no competing financial interest.

■ ACKNOWLEDGMENTS

This work was supported by NSF Grants CHE-1808239 and CHE-2108306/2108307 (C.R.B. and W.H.) and the National High Magnetic Field Laboratory's User Collaborative Grant Program, supported by the National Science Foundation Cooperative Agreement DMR-1644779* and the State of Florida.

■ REFERENCES

(1) Bowers, C. R.; Weitekamp, D. P. Parahydrogen and Synthesis Allow Dramatically Enhanced Nuclear Alignment. *J. Am. Chem. Soc.* **1987**, *109* (18), 5541−5542.
(2) Bowers, C. R.; Weitekamp, D. P. Transformation of Symmetrization Order to Nuclear-Spin Magnetization by Chemical Reaction and Nuclear Magnetic Resonance. *Phys. Rev. Lett.* **1986**, *57* (21), 2645−2648.
(3) Schmidt, A. B.; Hövener, J. B.; Bowers, C. R.; Buckenmaier, K.; Chekmenev, E. Y.; de Maissin, H.; Eills, J.; Ellermann, F.; Glöggler, S.; Gordon, J. W.; Knecht, S.; Koptyug, I. v.; Kuhn, J.; Pravdivtsev, A. N.; Reineri, F.; Theis, T.; Them, K. Instrumentation for Hydrogenative Parahydrogen-Based Hyperpolarization Techniques. *Anal. Chem.* **2022**, *94* (1), 479−502.
(4) Pokochueva, E.; Burueva, D.; Kovtunova, L.; Bukhtiyarov, A.; Gladky, A.; Kovtunov, K. v.; Koptyug, I. v.; Bukhtiyarov, V. Mechanistic in Situ Investigation of Heterogeneous Hydrogenation over Rh/TiO_2 Catalysts: Selectivity, Pairwise Route, Catalyst Nature. *Faraday Discuss.* **2021**, *229*, 161.
(5) Song, B.; Choi, D.; Xin, Y.; Bowers, C. R.; Hagelin-Weaver, H. Ultra-Low Loading Pt/CeO_2 Catalysts: Ceria Facet Effect Affords Improved Pairwise Selectivity for Parahydrogen Enhanced NMR Spectroscopy. *Angew. Chem., Int. Ed.* **2021**, *60* (8), 4038−4042.
(6) Panja, C.; Saliba, N. A.; Koel, B. E. Coking Resistance of Pt−Sn Alloys Probed by Acetylene Chemisorption. *Catal. Lett.* **2000**, *68* (3), 175−180.
(7) Panja, C.; Saliba, N. A.; Koel, B. E. Acetylene Chemisorption on Sn/Pt(100) Alloys. *J. Phys. Chem. B* **2001**, *105* (18), 3786−3796.
(8) Maligal-Ganesh, R. V.; Xiao, C.; Goh, T. W.; Wang, L.-L.; Gustafson, J.; Pei, Y.; Qi, Z.; Johnson, D. D.; Zhang, S.; Tao, F.; Huang, W. A Ship-in-a-Bottle Strategy To Synthesize Encapsulated Intermetallic Nanoparticle Catalysts: Exemplified for Furfural Hydrogenation. *ACS Catal.* **2016**, *6* (3), 1754−1763.
(9) Bariås, O. A.; Holmen, A.; Blekkan, E. A. Propane Dehydrogenation over Supported Pt and Pt−Sn Catalysts: Catalyst Preparation, Characterization, and Activity Measurements. *J. Catal.* **1996**, *158* (1), 1−12.
(10) Peck, J. W.; Mahon, D. I.; Koel, B. E. A Temperature Programmed Desorption Study of the Reaction of Methylacetylene on Pt(111) and Sn/Pt(111) Surface Alloys. *Surf. Sci.* **1998**, *410* (2), 200−213.
(11) Tsai, Y.-L.; Koel, B. E. Temperature-Programmed Desorption Investigation of the Adsorption and Reaction of Butene Isomers on Pt(111) and Ordered Pt−Sn Surface Alloys. *J. Phys. Chem. B* **1997**, *101* (15), 2895−2906.
(12) Zhao, H.; Koel, B. E. Influence of Coadsorbed Hydrogen on Ethylene Adsorption and Reaction on a $(\sqrt{3}\times\sqrt{3})$R30°-Sn/Pt(111) Surface Alloy. *Langmuir* **2005**, *21* (3), 971−975.
(13) Tsai, Y.-L.; Xu, C.; Koel, B. E. Chemisorption of Ethylene, Propylene and Isobutylene on Ordered Sn/Pt(111) Surface Alloys. *Surf. Sci.* **1997**, *385* (1), 37−59.
(14) Zhao, H.; Koel, B. E. Reactivity of Ethyl Groups on a Sn/Pt(111) Surface Alloy. *Catal. Lett.* **2005**, *99* (1), 27−32.
(15) Batzill, M.; Beck, D. E.; Koel, B. E. Electronic Contrast in Scanning Tunneling Microscopy of Sn−Pt(111) Surface Alloys. *Surf. Sci.* **2000**, *466* (1), L821−L826.
(16) Yang, M.-L.; Zhu, Y.-A.; Zhou, X.-G.; Sui, Z.-J.; Chen, D. First-Principles Calculations of Propane Dehydrogenation over PtSn Catalysts. *ACS Catal.* **2012**, *2* (6), 1247−1258.
(17) Yang, M. L.; Zhu, Y. A.; Fan, C.; Sui, Z. J.; Chen, D.; Zhou, X. G. Density Functional Study of the Chemisorption of C1, C2 and C3 Intermediates in Propane Dissociation on Pt(1 1 1). *J. Mol. Catal. A: Chem.* **2010**, *321*, 42.
(18) Nykänen, L.; Honkala, K. Density Functional Theory Study on Propane and Propene Adsorption on Pt(111) and PtSn Alloy Surfaces. *J. Phys. Chem. C* **2011**, *115* (19), 9578−9586.
(19) Pei, Y.; Maligal-Ganesh, R. v.; Xiao, C.; Goh, T.-W.; Brashler, K.; Gustafson, J. A.; Huang, W. An Inorganic Capping Strategy for the Seeded Growth of Versatile Bimetallic Nanostructures. *Nanoscale* **2015**, *7* (40), 16721−16728.
(20) Zhao, E. W.; Maligal-Ganesh, R.; Du, Y.; Zhao, T. Y.; Collins, J.; Ma, T.; Zhou, L.; Goh, T. W.; Huang, W.; Bowers, C. R. Surface-Mediated Hyperpolarization of Liquid Water from Parahydrogen. *Chem.* **2018**, *4* (6), 1387−1403.
(21) Zhao, E. W.; Maligal-Ganesh, R.; Xiao, C.; Goh, T.-W. W.; Qi, Z.; Pei, Y.; Hagelin-Weaver, H. E.; Huang, W.; Bowers, C. R. Silica-Encapsulated Pt-Sn Intermetallic Nanoparticles: A Robust Catalytic Platform for Parahydrogen-Induced Polarization of Gases and Liquids. *Angew. Chem.* **2017**, *129* (14), 3983−3987.
(22) Fearon, J.; Watson, G. W. Hydrogen Adsorption and Diffusion on Pt {111} and PtSn {111. *J. Mater. Chem.* **2006**, *16* (20), 1989−1996.
(23) Voss, M. R.; Busse, H.; Koel, B. E. Adsorption of Thermal D Atoms on Sn/Pt(111) Surface Alloys. *Surf. Sci.* **1998**, *414* (3), 330−340.
(24) Samson, P.; Nesbitt, A.; Koel, B. E.; Hodgson, A. Deuterium Dissociation on Ordered Sn/Pt(111) Surface Alloys. *J. Chem. Phys.* **1998**, *109* (8), 3255−3264.
(25) Zhivonitko, V. v.; Skovpin, I. v.; Szeto, K. C.; Taoufik, M.; Koptyug, I. v. Parahydrogen-Induced Polarization Study of the Silica-Supported Vanadium Oxo Organometallic Catalyst. *J. Phys. Chem. C* **2018**, *122* (9), 4891−4900.
(26) Skovpin, I. V.; Zhivonitko, V. V.; Kaptein, R.; Koptyug, I. V. Generating Parahydrogen-Induced Polarization Using Immobilized Iridium Complexes in the Gas-Phase Hydrogenation of Carbon-Carbon Double and Triple Bonds. *Appl. Magn. Reson.* **2013**, *44* (1−2), 289−300.
(27) Kovtunov, K. v.; Beck, I. E.; Zhivonitko, V. v.; Barskiy, D. A.; Bukhtiyarov, V. I.; Koptyug, I. v. Heterogeneous Addition of H2 to Double and Triple Bonds over Supported Pd Catalysts: A Parahydrogen-Induced Polarization Technique Study. *Phys. Chem. Chem. Phys.* **2012**, *14* (31), 11008−11014.
(28) Pravica, M. G.; Weitekamp, D. P. Net NMR Alignment by Adiabatic Transport of Parahydrogen Addition Products to High Magnetic Field. *Chem. Phys. Lett.* **1988**, *145* (4), 255−258.
(29) Kovtunov, K. v.; Salnikov, O. G.; Zhivonitko, V. v.; Skovpin, I. v.; Bukhtiyarov, V. I.; Koptyug, I. v. Catalysis and Nuclear Magnetic Resonance Signal Enhancement with Parahydrogen. *Top. Catal.* **2016**, *59* (19), 1686−1699.
(30) Bengs, C.; Levitt, M. H. SpinDynamica: Symbolic and Numerical Magnetic Resonance in a Mathematica Environment. *Magn. Reson. Chem.* **2018**, *56* (6), 374−414.
(31) Zhou, R.; Cheng, W.; Neal, L. M.; Zhao, E. W.; Ludden, K.; Hagelin-Weaver, H. E.; Bowers, C. R. Parahydrogen Enhanced NMR Reveals Correlations in Selective Hydrogenation of Triple Bonds over Supported Pt Catalyst. *Phys. Chem. Chem. Phys.* **2015**, *17* (39), 26121−26129.
(32) Busse, H.; Voss, M. R.; Jerdev, D.; Koel, B. E.; Paffett, M. T. Adsorption and Reaction of Gaseous H(D) Atoms with D(H) Adatoms on Pt(111) and Sn/Pt(111) Surface Alloys. *Surf. Sci.* **2001**, *490* (1), 133−143.
(33) Bond, G. C.; Webb, G.; Wells, P. B.; Winterbottom, J. M. Patterns of Behavior in Catalysis by Metals. *J. Catal.* **1962**, *1* (1), 74−84.

https://doi.org/10.1021/acs.jpclett.2c00581
J. Phys. Chem. Lett. 2022, 13, 4125−4132

(34) Teschner, D.; Borsodi, J.; Wootsch, A.; Révay, Z.; Hävecker, M.; Knop-Gericke, A.; Jackson, S. D.; Schlögl, R. The Roles of Subsurface Carbon and Hydrogen in Palladium-Catalyzed Alkyne Hydrogenation. *Science (1979)* **2008**, *320* (5872), 86−89.
(35) Kennedy, D. R.; Webb, G.; Jackson, S. D.; Lennon, D. Propyne Hydrogenation over Alumina-Supported Palladium and Platinum Catalysts. *Applied Catalysis A: General* **2004**, *259* (1), 109−120.
(36) Kennedy, D. R.; Cullen, B.; Lennon, D.; Webb, G.; Dennison, P. R.; Jackson, S. D. Propyne Hydrogenation over a Silica-Supported Platinum Catalyst Studied under Transient Conditions. *Stud. Surf. Sci. Catal.* **1999**, *122*, 125−132.
(37) Sun, C.; Luo, J.; Cao, M.; Zheng, P.; Li, G.; Bu, J.; Cao, Z.; Chen, S.; Xie, X. A Comparative Study on Different Regeneration Processes of Pt-Sn/Γ-Al2O3 Catalysts for Propane Dehydrogenation. *Journal of Energy Chemistry* **20182018**, *27* (1), 311−318.
(38) Pham, H. N.; Sattler, J. J. H. B.; Weckhuysen, B. M.; Datye, A. K. Role of Sn in the Regeneration of Pt/γ-Al2O3 Light Alkane Dehydrogenation Catalysts. *ACS Catal.* **2016**, *6* (4), 2257−2264.
(39) Deng, L.; Zhou, Z.; Shishido, T. Behavior of Active Species on Pt-Sn/SiO_2 Catalyst during the Dehydrogenation of Propane and Regeneration. *Applied Catalysis A: General* **2020**, *606*, 117826.
(40) Afonso, J. C.; Aranda, D. A. G.; Schmal, M.; Frety, R. Regeneration of a Pt-Sn/Al2O3 Catalyst: Influence of Heating Rate, Temperature and Time of Regeneration. *Fuel Process. Technol.* **1997**, *50* (1), 35−48.
(41) Afonso, J. C.; Aranda, D. A. G.; Schmal, M.; Frety, R. Importance of Pretreatment on Regeneration of a Pt-Sn/Al2O3 Catalyst. *Fuel Process. Technol.* **1995**, *42* (1), 3−17.
(42) Iglesias-Juez, A.; Beale, A. M.; Maaijen, K.; Weng, T. C.; Glatzel, P.; Weckhuysen, B. M. A Combined in Situ Time-Resolved UV-Vis, Raman and High-Energy Resolution X-Ray Absorption Spectroscopy Study on the Deactivation Behavior of Pt and PtSn Propane Dehydrogenation Catalysts under Industrial Reaction Conditions. *J. Catal.* **2010**, *276* (2), 268−279.
(43) Argyle, M. D.; Bartholomew, C. H. Heterogeneous Catalyst Deactivation and Regeneration: A Review. *Catalysts. MDPI AG February* **2015**, *26*, 145−269.
(44) Choi, Y. S.; Oh, K.; Jung, K.-D.; Kim, W.-I.; Koh, H. L. Regeneration of Pt-Sn/Al2O3 Catalyst for Hydrogen Production through Propane Dehydrogenation Using Hydrochloric Acid. *Catalysts* **2020**, *10* (8), 898.
(45) Bond, G. C. *Metal-Catalysed Reactions of Hydrocarbons*; Springer: 2005.
(46) Jin, Y.; Datye, A. K; Rightor, E.; Gulotty, R.; Waterman, W.; Smith, M.; Holbrook, M.; Maj, J.; Blackson, J. The Influence of Catalyst Restructuring on the Selective Hydrogenation of Acetylene to Ethylene. *J. Catal.* **2001**, *203* (2), 292−306.
(47) Zhou, R.; Zhao, E. W.; Cheng, W.; Neal, L. M.; Zheng, H.; Quinones, R. E.; Hagelin-Weaver, H. E.; Bowers, C. R. Parahydrogen-Induced Polarization by Pairwise Replacement Catalysis on Pt and Ir Nanoparticles. *J. Am. Chem. Soc.* **2015**, *137* (5), 1938−1946.

https://doi.org/10.1021/acs.jpclett.2c00581
J. Phys. Chem. Lett. 2022, 13, 4125−4132